Soft Matter

Cellulose Nanocrystals for Gelation and Percolation-induced Reinforcement of a Photocurable Poly (vinyl alcohol) Derivative

Journal:	*Soft Matter*
Manuscript ID	SM-ART-07-2020-001376.R1
Article Type:	Paper
Date Submitted by the Author:	16-Aug-2020
Complete List of Authors:	Corder, Ria; North Carolina State University, Chemical and Biomolecular Engineering Adhikari, Prajesh; North Carolina State University, Chemical and Biomolecular Engineering Burroughs, Michael; North Carolina State University, Chemical and Biomolecular Engineering Rojas, Orlando; Aalto University, Bioproducts and Biosystems, School of Chemical Engineering; The University of British Columbia, Chemical and Biological Engineering Khan, Saad; North Carolina State University, Chemical and Biomolecular Engineering

Cellulose Nanocrystals for Gelation and Percolation-induced Reinforcement of a Photocurable Poly (vinyl alcohol) Derivative

Ria D. Corder,[1*] Prajesh Adhikari,[1*] Michael C. Burroughs,[1†] Orlando J. Rojas,[1,2,3‡] and Saad A. Khan[1‡]

[1]Department of Chemical and Biomolecular Engineering, North Carolina State University, Raleigh, NC 27695, USA

[2]Department of Bioproducts and Biosystems, School of Chemical Engineering, Aalto University, Espoo, FI-00076, Finland

[3]Bioproducts Institute, Department of Chemical and Biological Engineering, Chemistry and Wood Science, University of British Columbia, Vancouver BC V6T 1Z3, Canada

ABSTRACT

Nanomaterials are regularly added to crosslinkable polymers to enhance mechanical properties; however, important effects related to gelation behavior and crosslinking kinetics are often overlooked. In this study, we combine cellulose nanocrystals (CNCs) with a photoactive poly (vinyl alcohol) derivative, PVA-SbQ, to form photocrosslinked nanocomposite hydrogels. We investigate the rheology of PVA-

* Co-first authors.

† Current address: Department of Chemical Engineering, University of California Santa Barbara, Santa Barbara, CA, 93106.

‡ Corresponding authors (email: orlando.rojas@ubc.ca; khan@eos.ncsu.edu).

SbQ with and without CNCs to decipher the role of each component in final property development and identify a critical CNC concentration (1.5 wt%) above which several changes in rheological behavior are observed. Neat PVA-SbQ solutions exhibit Newtonian flow behavior across all concentrations, while CNC dispersions are shear-thinning <6 wt% and gel at high concentrations. Combining semi-dilute entangled PVA-SbQ (6 wt%) with >1.5 wt% CNCs forms a percolated microstructure. *In-situ* photocrosslinking experiments reveal how CNCs affect both the gelation kinetics and storage modulus (G') of the resulting hydrogels. The modulus crossover time increases after addition of up to 1.5 wt% CNCs, while no modulus crossover is observed >1.5 wt% CNCs. A sharp increase in G' is observed >1.5 wt% CNCs for fully-crosslinked networks due to favorable PVA-SbQ/CNC interactions. A percolation model is fitted to the G' data to confirm that mechanical percolation is maintained after photocrosslinking. A ~120% increase in G' for 2.5 wt% CNCs (relative to neat PVA-SbQ) confirms that CNCs provide a reinforcing effect through the percolated microstructure formed from CNC-polymer interactions. The results are testament to the ability of CNCs to significantly alter the

storage moduli of crosslinked polymer gels at low loading fractions through percolation-induced reinforcement.

KEYWORDS

cellulose nanocrystal, photocrosslinking, percolation, rheology, gelation

INTRODUCTION

The formation of three-dimensional polymer networks for applications such as coatings,[1,2] adhesives,[3,4] tissue engineering,[5] and 3D printing[6–8] has been realized through the use of synthetic polymers such as poly (vinyl alcohol) (PVA),[9,10] poly (ethylene glycol),[11,12] and poly (acrylic acid)[13,14] as well as natural biopolymers such as cellulose,[15–18] chitosan,[19,20] gelatin,[21] and alginates.[22] These networks are typically formed by either physical crosslinking *via* ionic or hydrogen bonding, or by chemical crosslinking using free radical, “click” chemistry, or photopolymerization techniques.[23] Typically, photocrosslinkable systems consist of monomers or oligomers, photoinitiators, and often additional crosslinking agents that undergo a series of radical generation and monomer addition steps in the presence of UV light to form highly insoluble, interconnected 3D architectures.[24,25] Many common photoinitiators, such as benzophenone, accumulate in the environment and have adverse effects on human health,[26] while the presence of unreacted crosslinking agents in a crosslinked gel network can have a plasticizing effect[27] and reduce performance.[28] In this regard, polymers with inherent photosensitivity, containing light-sensitive photocrosslinkable

moieties that undergo rapid intermolecular crosslinking upon exposure to light, are attractive additions to the library of photocrosslinkable polymer systems which allow for reduced energy consumption relative to thermally-cured systems[29] without the need for additional photoinitiators or crosslinking agents.

One such commercially available, water-soluble, photocrosslinkable polymer of interest is PVA containing styrylpyridium side chains (PVA-SbQ), which is synthesized via substitution of pendant hydroxyl groups on the PVA backbone with a photoactive SbQ moiety.[30–33] The addition of small amounts of SbQ (0.1-4 mol%) to the PVA backbone offers very high photosensitivity relative to conventional photoresists[30,31] while maintaining the beneficial characteristics of PVA such as biocompatibility and gas barrier properties. Photodimerization of double bonds in the presence of UV light (λ ~ 365 nm) produces a 3D structure that partially swells but does not disassociate in aqueous solutions. Using quartz crystal microgravimetry (QCM), Bai *et al.*[34] observed that the shifts in QCM frequency and energy dissipation upon photodimerization of SbQ moieties correlate with a three-stage transition from a soft viscoelastic material to a rigid film. PVA-SbQ has been used to immobilize proteins,[34–37] for cell entrapment,[38] as a

crosslinker in systems containing hyaluronic acid,[39] and in photopolymer emulsions for screen-printing and bio-printable ink formulations.[32] However, these systems are often limited by weak mechanical performance, requiring further reinforcement.

Several strategies have been utilized to increase the strength of crosslinked networks including the inclusion of nanoparticles[40–42] and the formation of double[43] and interpenetrating[44,45] networks. Herein, we report on biodegradable, rod-like cellulose nanocrystals (CNCs) to achieve mechanical reinforcement of PVA-SbQ *via* a percolation mechanism. CNCs can spontaneously self-organize into a chiral nematic liquid crystal phase above an onset concentration[46] and can form physical gels beyond a critical concentration due to loss of colloidal stability and the formation of a percolated network.[47] Gels can also be formed by combining CNCs with adsorbing and/or non-adsorbing polymers. For instance, Boluk *et al.*[48] investigated the interactions of CNCs with two water-soluble polymers, non-ionic hydroxyethyl cellulose and ionic carboxymethyl cellulose, using viscoelastic rheological measurements and isothermal titration calorimetry. They revealed the formation of weak gels exhibiting yield stresses, which was attributed to depletion flocculation due to the presence of non-adsorbing

polymers.[48] Small amounts of adsorbing polymers such as non-ionic polysaccharides, which increased the effective volume fraction of CNC dispersions, were found to lower the CNC concentration required for gelation.[49] Using QCM analysis, the interactions of two water-soluble polymers (anionic sodium polyacrylate (PAAS) and non-ionic polyethylene glycol (PEG)) were explored on the self-assembly behavior of commercial CNC suspensions.[50] It was revealed that PEG adsorbs onto CNCs, due to steric stabilization and hydrogen bonding between CNCs and PEG, but that PAAS does not adsorb onto CNCs due to unfavorable electrostatic interactions.[50] Depletion flocculation has been identified as primary reason for CNC gelation in semi-dilute, unentangled carboxymethyl cellulose solutions, whereas weak depletion interactions occurred in systems with poly(ethylene oxide) (PEO) after surfaces were saturated with adsorbed PEO.[51] Cohen *et al.*[52] used small-angle X-ray scattering to reveal that at high polymer concentrations, solvated PVA chains disrupt the self-assembly of CNCs into chiral nematic phases while poly(vinylpyrrolidone) does not affect CNC assembly, suggesting that the specific structure of the polymers (rather than depletion interactions or physical properties) govern the phase behavior of polymer-CNC mixtures. CNCs have recently

been incorporated into polymer nanocomposites to augment the mechanical performance of natural rubber latex,[53] epoxy resins,[54] collagen hydrogels,[55] and 3D-printed PEG-based hydrogels.[56] The level of system complexity is further increased when fillers are incorporated within a photocrosslinkable system, as factors such as UV light intensity and irradiation time can affect how fillers interfere with incipient polymer network formation and alter the gelation kinetics or mechanism, making each system appear to behave uniquely unto itself.[57,58] So, while photogelation of filled systems can provide an elegant method to achieving enhanced properties, there is a critical need to understand how fillers affect mechanical property development.

In this work, we combine photocrosslinkable PVA-SbQ and CNCs (**Scheme 1**) to form mechanically-reinforced photocurable networks in the absence of external photoinitiators or crosslinking agents. The presence of negatively-charged CNC in aqueous solutions of positively-charged PVA-SbQ induces attractive electrostatics. We observe that CNCs form a percolated microstructure in PVA-SbQ solutions beyond a critical concentration. *In-situ* photocuring experiments reveal that the percolation of CNCs is maintained after photocrosslinking of PVA-SbQ, leading to higher storage

moduli. The effect of CNC addition on gelation kinetics is also characterized. This study advances the understanding and development of photocurable polymer nanocomposite systems for potential applications as functional hydrogels, such as but not limited to UV-based gel spinning and 3D printing.

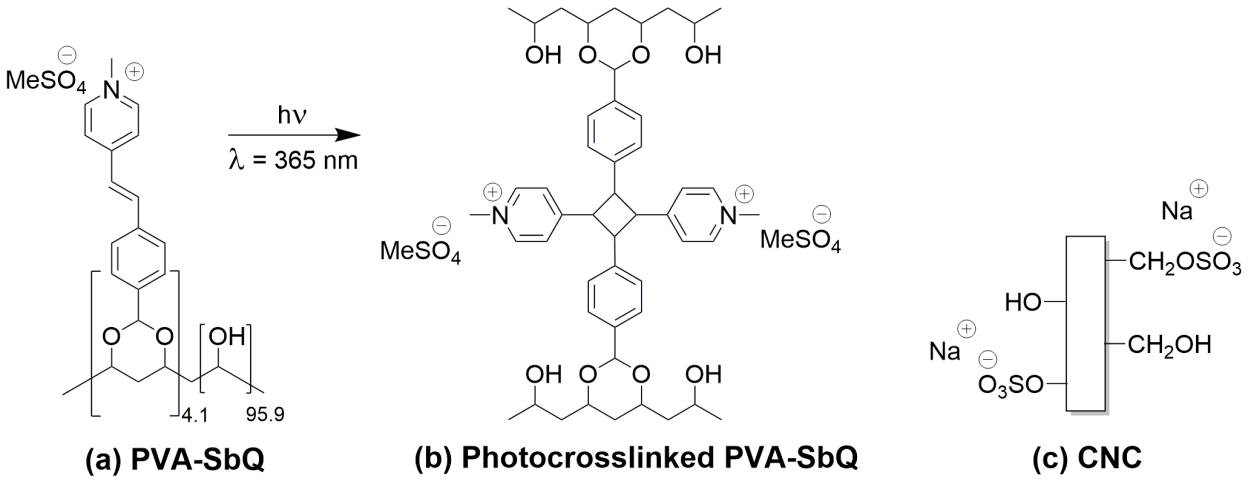

(a) PVA-SbQ **(b) Photocrosslinked PVA-SbQ** **(c) CNC**

Scheme 1. (a) Chemical structures of PVA-SbQ, 4.1 mol% SbQ content) and (b) photocrosslinked PVA-SbQ, and (c) surface functionality of CNC containing sulfate half ester groups and sodium counterions.

EXPERIMENTAL SECTION

Materials. Poly (vinyl alcohol), N-methyl-4 (4'-formylstyrl) pyridinium methosulfate acetal (PVA-SbQ, MW ~ 45,000 g/mol and 4.1 mol% SbQ content, 13.3 wt% in water, Polysciences Inc., Warrington, PA) and cellulose nanocrystals (CNCs, length of 100 nm, width of 5 nm, produced in the USDA Forest Products Lab, Wisconsin and acquired from the University of Maine Process Development Center) were used as received. Prior to preparing dispersions, CNC powder was dried in a vacuum oven for 2 days at 120 ˚C.

Preparation of PVA-SbQ/CNC dispersions. A 5 wt% homogeneous stock dispersion of CNCs in deionized (DI) water was prepared by adding DI water to the dried CNCs, and vortex mixing for 1-2 minutes to break down large aggregates. After vortex mixing, the aqueous CNC dispersion was placed in a bath sonicator (8510 Ultrasonic Cleaner, Branson) for 4 hours at 4°C to prevent temperature-induced artifacts such as aggregation and reverse esterification. Following sonication, the visually homogeneous CNC dispersion was stored in a refrigerator at 4 °C. After 30 days, there was no evidence of CNCs settling. Aqueous solutions of PVA-SbQ containing well-dispersed CNCs were made by combining the stock solutions of aqueous CNC and

PVA-SbQ and diluting to the desired levels with DI water, followed by 30 seconds of vortex mixing. Afterwards, the vials were wrapped in aluminum foil to prevent trace UV light exposure and placed on a stir plate for 6 hours. Following stirring, the PVA-SbQ/CNC dispersions were sonicated for 1 hour and were then stored in a refrigerator at 4 °C. Samples were taken out of the refrigerator and stirred for 40 minutes at room temperature prior to any experiments. All experiments were completed within 7 days of sample preparation.

Dispersion characterization. Particle size, electrophoretic mobility, zeta potential, and conductivity measurements of aqueous CNC dispersions with and without PVA-SbQ were obtained using a Zetasizer 2000 (Malvern Instruments) equipped with a 4.0 mW He-Ne laser (λ = 633 nm). Electrophoretic mobilities were converted to zeta potentials following the Smoluchowski theory.[59] Reported values are average of six independent measurements.

Rheological measurements. All rheological experiments were performed at room temperature using a Discovery Hybrid Rheometer-2 (TA Instruments). A 20 mm aluminum parallel plate top geometry and a sample gap of 500 μm were used for all

experiments. To ensure consistency across samples, measurements were performed after pre-shearing samples at ω = 10 rad/s for 10 s followed by 10 s of equilibration time. Steady-shear experiments were performed on PVA-SbQ solutions, CNC dispersions, and PVA-SbQ solutions containing dispersed CNCs by sweeping through a range of increasing shear rates (exact range varied with sample type). Dynamic oscillatory experiments were performed on PVA-SbQ solutions containing dispersed CNCs both before and after photocrosslinking over an oscillatory frequency (ω) range of 10^{-2}-10^{2} rad/s. Before conducting dynamic experiments, stress sweeps were performed to ensure that the oscillation stress selected for each sample would be within its corresponding linear viscoelastic regime. The UV LED accessory (TA Instruments), equipped with a transparent acrylic bottom plate, was used to administer controlled dosages of UV light (λ = 365 nm) to each sample during photocrosslinking experiments. A UV radiometer (Silver Line) was used to calibrate the intensity of UV light before each experiment. Samples were continuously exposed to UV light with an intensity of 10 mW/cm^2 for the duration of each oscillatory time sweep. The onset of UV light exposure was synchronized with the beginning of each oscillatory time sweep. The frequency of

dynamic oscillation was fixed at 10 rad/s throughout the duration of each time sweep.

RESULTS AND DISCUSSION

PVA-SbQ solution rheology. Understanding the precise mechanism by which CNCs alter rheological behavior of PVA-SbQ relies first on the determination of whether aqueous PVA-SbQ solutions behave rheologically as neutral polymers or as polyelectrolytes, and then on the determination of the entanglement regime using simple steady shear rheology combined with scaling principles. In the semi-dilute unentangled and semi-dilute entangled regimes for neutral polymers, the apparent viscosity (η) scales with concentration to the 2 and 4.7 powers, respectively,[60] in sharp contrast to polyelectrolytes for which viscosity scales with concentration to 0.5 and 1.5 powers.[61,62] The effect of PVA-SbQ concentration (2-10 wt%) on the steady-shear rheology over three decades of shear rate (10^0-10^3 s^{-1}) is presented in **Figure 1a**. At low concentrations (< 2 wt%), the viscosity of PVA-SbQ is close to that of water (10^{-3} Pa-s). Viscosity increases with increasing concentration of PVA-SbQ and is over two orders of magnitude higher at 10 wt% as compared to 2 wt%. Typically, polymer solutions exhibit

shear-thinning behavior[63] at elevated shear rates; however, PVA-SbQ solutions maintain Newtonian flow behavior (constant η over all shear rates) irrespective of polymer concentration. This observed Newtonian flow behavior over a wide shear rate range may be in part due to the relatively high molecular weight of the PVA-SbQ used in this work; similar Newtonian flow behavior has previously been observed for semi-dilute PVA solutions.[64] The specific viscosity (η_{sp}) of each PVA-SbQ solution was calculated according to Equation 1:

$$\eta_{sp} = \frac{\eta - \eta_s}{\eta_s} \qquad (1)$$

where η is the Newtonian viscosity (calculated by averaging η values across all applied shear rates) and η_s is the viscosity of the solvent (10^{-3} Pa-s). From the log-log plot of η_{sp} versus polymer concentration presented in **Figure 1b**, scaling relationships between η_{sp} and polymer concentration along with the entanglement concentration (C_e) can be determined. **Figure 1b** reveals slopes of 2.2 and 4.9 for the semi-dilute unentangled and semi-dilute entangled regimes, which are in excellent agreement with scaling relationships for neutral polymers.[60] While PVA-SbQ contains small amounts (4.1 mol%)

of positively-charged N-methyl-4(4'-formylstyrl) pyridinium methosulfate acetal groups, the charge density is not sufficient to impart polyelectrolyte characteristics. The experimentally determined C_e, taken as the line intersection of the two power law scaling profiles in **Figure 1b**, is ~ 4.8 wt%.

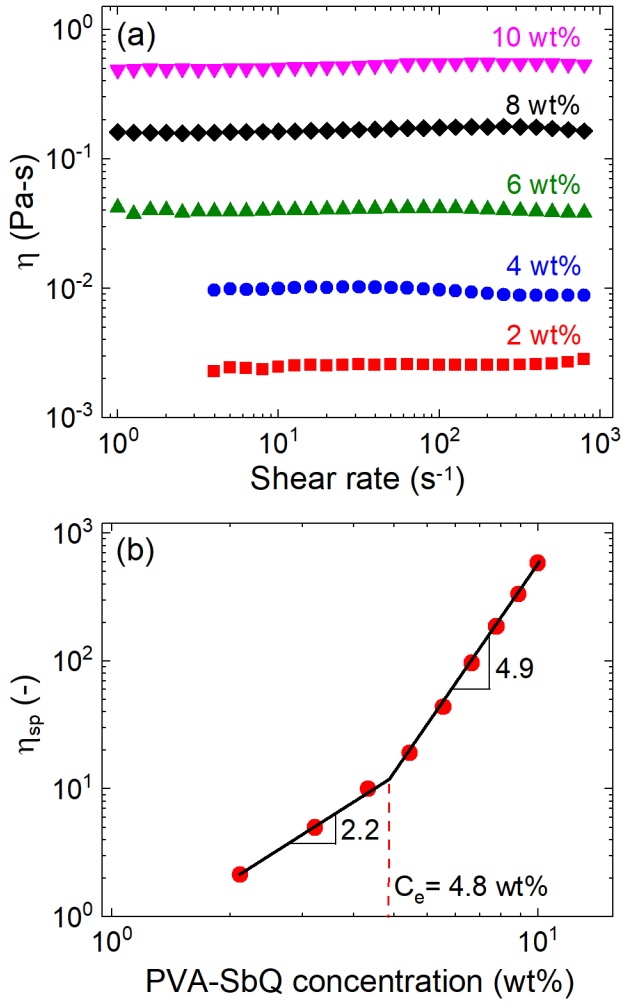

Figure 1. (a) Steady shear viscosity (η) data as a function of shear rate for varying

concentrations of PVA-SbQ in DI water (data sets labeled and color-coded). (b) Specific viscosity (η_{sp}) of PVA-SbQ solutions. The black lines are power-law fits to the data. The line intersection is used to estimate C_e.

Dispersion properties of CNCs in DI water and with PVA-SbQ. The physical properties of CNC used in this work, as well its surface characteristics, have been characterized thoroughly.[50] The hydrodynamic characteristics of 0.1 and 0.5 wt% CNCs dispersed in DI water are presented in **Table 1**. 0.1 wt% CNCs display a hydrodynamic size of 90.7 ± 0.4 nm and a zeta potential of -42.8 ± 2.2 mV, with the negative zeta potential arising due to negative surface charges (**Scheme 1**). The theoretical hydrodynamic size for CNCs of length 100 nm and aspect ratio (≡ particle length/width) of 25, calculated using combinations of the Stokes-Einstein equation and Kirkwood-Riseman theory[65] is 16.7 nm, suggesting that CNCs are not individually dispersed but show appreciable aggregation. Details of this calculation are provided in the **Supporting Information**. CNCs remain highly dispersed and negatively charged when the concentration is increased to 0.5 wt%, with a hydrodynamic size of 69.8 ± 0.7 nm and a

zeta potential of -53.6 ± 4.9 mV. Slight variations in the size and zeta potential between the two CNC concentrations are likely due to the non-spherical shape of CNCs.[66] The increase in CNC concentration also increases the solution conductivity from 0.037 ± 0.002 to 0.080 ± 0.002 mS/cm, as reported in **Table 1.**

Table 1. Hydrodynamic size, electrophoretic mobility, zeta potential, and conductivity of 0.1 wt% and 0.5 wt% CNCs dispersed in deionized (DI) water and in a 0.45 wt% (100 μM) PVA-SbQ solution.

	0.1 wt% CNCs		0.5 wt% CNCs	
Dispersed in	*DI water*	*PVA-SbQ*	*DI water*	*PVA-SbQ*
Size (nm)	90.7 ± 0.4	348.7 ± 6.2	69.8 ± 0.7	149.7 ± 1.7
Mobility (μM.cm/V.s)	-3.36 ± 0.17	1.74 ± 0.13	-4.20 ± 0.39	-2.62 ± 0.03
Zeta potential (mV)	-42.8 ± 2.2	22.2 ± 1.6	-53.6 ± 4.9	-33.5 ± 0.3
Conductivity (mS/cm)	0.037 ± 0.002	0.080 ± 0.002	0.080 ± 0.002	0.126 ± 0.005

The interactions between dilute CNC dispersions and PVA-SbQ were further studied through hydrodynamic experiments. The hydrodynamic size and zeta potential of the 0.1 wt% CNC dispersion increased from 90.7 ± 0.4 nm and 42.8 ± 2.2 mV

respectively to 348.7 ± 6.2 nm and 22.2 ± 1.6 mV upon addition of 0.45 wt% (100 μM) PVA-SbQ (**Table 1**). The increase in hydrodynamic size and switch to a positive zeta potential implies aggregated structures are stabilized by excess PVA-SbQ; this is visibly apparent from the increase in solution turbidity upon addition of PVA-SbQ (**Figure S1)**. Similarly, for dispersions containing 0.5 wt% CNCs, the initial hydrodynamic size and zeta potential of increased from 69.8 ± 0.7 nm and -53.6 ± 4.9 mV to 149.7 ± 1.7 nm and -33.5 ± 0.3 mV respectively after addition of 100 μM PVA-SbQ (**Table 1**), forming visibly aggregated structures with net negative charges (**Figure S1**).

We proceed to further examine the rheological behavior of CNCs as an extension of previous work done by several researchers. Images of CNC dispersions in water at concentrations between 0.1 and 10 wt% are shown in **Figure 2**, where vial inversion tests indicate a transition from solution-like to gel-like behavior at concentrations between 6 and 6.7 wt% CNC. The concentration of CNCs used in this work to form PVA-SbQ composites was limited to < 2.5 wt%, well within the solution-like regime.

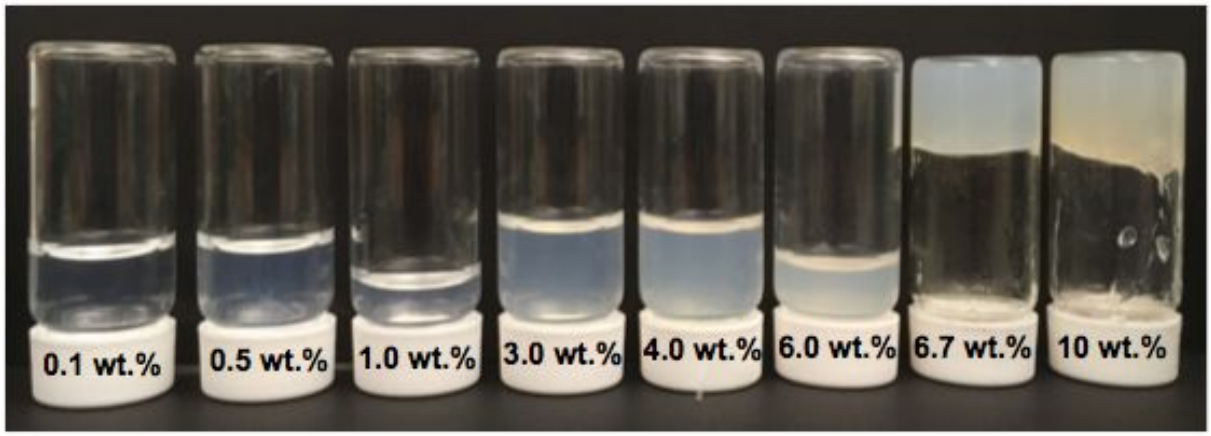

Figure 2. Images of aqueous CNC dispersions at varying wt% in DI water in 7 mL scintillation vials.

Steady-shear viscosity data for CNC dispersions is displayed in **Figure S2**. CNC contributions to viscosity in the dilute regime can then be used to determine their aspect ratio, which otherwise is typically determined using microscopy techniques. The intrinsic viscosity of CNCs is estimated to be 47 mL/g (using a Huggins plot as shown in **Figure S3**) due to extra energy dissipation arising from non-spherical nature of particles.[67] Using Simha's equation, which captures the effect of particle shape on intrinsic viscosity, the CNC aspect ratio is estimated to be ~26,[68,69] which is in excellent agreement with the manufacturer-reported dimensions of CNCs. Details of this calculation are provided in the **Supporting Information**.

Rheology of PVA-SbQ combined with CNCs. With the C_e of PVA-SbQ determined to be 4.8 wt%, rheological measurements on solutions with varying amounts of CNCs were performed to study the influence of CNCs on the microstructure and the photocrosslinking dynamics of entangled PVA-SbQ (6 wt%). The storage modulus (G') and loss modulus (G"), as well as complex viscosity (η*), as functions of frequency for PVA-SbQ containing varying amounts of CNCs are presented in **Figure 3**. For polymers in the terminal regime, G' ~ ω^2 and G" ~ ω. As shown in **Figure 3a**, 1 wt% CNCs with PVA-SbQ exhibits solution-like behavior (G' < G" and both moduli dependent on frequency). At a CNC loading of 1.5 wt%, G' is similar to G" in value, which is now substantially larger and both moduli exhibit a similar degree of frequency-dependence. Gel-like behavior (G' > G" and both moduli relatively independent of frequency over the applied frequency range) is observed for 2.5 wt% CNCs due to favorable polymer-CNC interactions forming sample-spanning, interconnected structures. The complex viscosity data for PVA-SbQ mixed with CNCs (**Figure 3b**) further support the frequency sweep results (**Figure 3a**). For PVA-SbQ with 1 wt% CNCs, a plateau in η* at low frequency is observed with weak shear-thinning occurring at higher frequency. A greater degree of

shear-thinning behavior is observed at and above 1.5 wt% CNCs. The frequency sweep and complex viscosity data for 0 and 2 wt% CNCs with 6 wt% PVA-SbQ have been omitted from **Figure 3** for the sake of clarity but are presented in **Figure S4**.

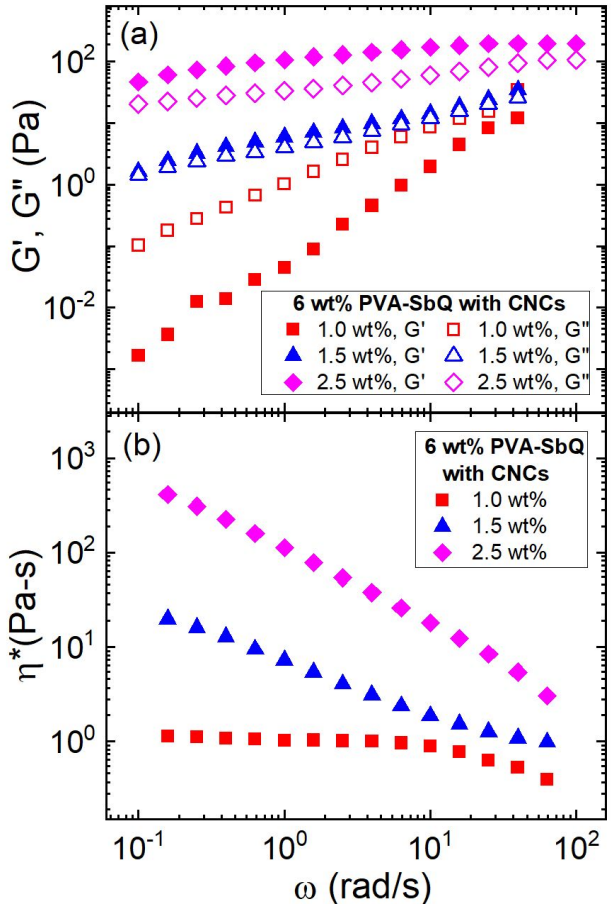

Figure 3. (a) Storage and loss moduli (filled symbols = G' and open symbols = G") and (b) complex viscosity (η*) versus frequency (ω), for 6 wt% PVA-SbQ containing CNCs up to 2.5 wt% (data sets labeled and color-coded).

The flow behavior index (n) can be extracted from the slope of η* using the scaling relationship $\eta^* \sim \omega^{n-1}$ above an onset frequency required for shear-thinning. Complete parameter fits to this power-law model are provided in **Table S1**. Values of n vary from 0.747 for neat PVA-SbQ down to 0.348 for 2.5 wt% CNCs with PVA-SbQ, with lower n-values indicating a greater degree of shear-thinning behavior. Measurements of shear stress (τ) vs shear rate (presented in **Figure S5**) reveal the presence of a yield stress at CNC concentrations above 1.5 wt%, matching the transition to shear-thinning behavior observed in **Figure 3b** attributed to a transformation from liquid-like to gel-like structures containing interconnected networks, often seen in filled polymer nanocomposites containing carbon nanotubes.[70–72] The resulting parameter fits of the Hershel-Bulkley model are presented in **Table S2**.

While the presence of a yield stress suggests the existence of interconnected structures, further analysis is necessary to validate the presence of microstructural ordering. The effect of nanofillers such as CNCs on polymer dynamics and the extent of interconnected structure formation can be studied by probing changes in rheological

parameters such as G', G", phase angle (δ), and complex modulus (G*) at low frequency. Two important plots, namely, van Gurp-Palmen and Cole-Cole plots, are very sensitive to the formation of interconnected structures in systems containing nanofillers in both polymeric solutions and melts and are often used as signatures for identification of a rheological percolation threshold. A van Gurp-Palmen plot shows the dependence of δ on |G*|, where a decrease in δ below 45^{o} is used as the criteria for percolation (the threshold filler concentration at which a transition from a liquid-like to solid-like microstructure occurs). A Cole-Cole plot shows the dependence of G' on G", with deviations from the original slope of systems without nanofillers representative of the formation of interconnected networks. These techniques have been used in prior literature to identify percolation thresholds, most notably for systems of CNC-filled polylactic acid[73,74] and carbon nanotube-based composites.[75] By analyzing both of these types of plots as a function of CNC loading, we can estimate the rheological percolation threshold for CNCs in 6 wt% PVA-SbQ.

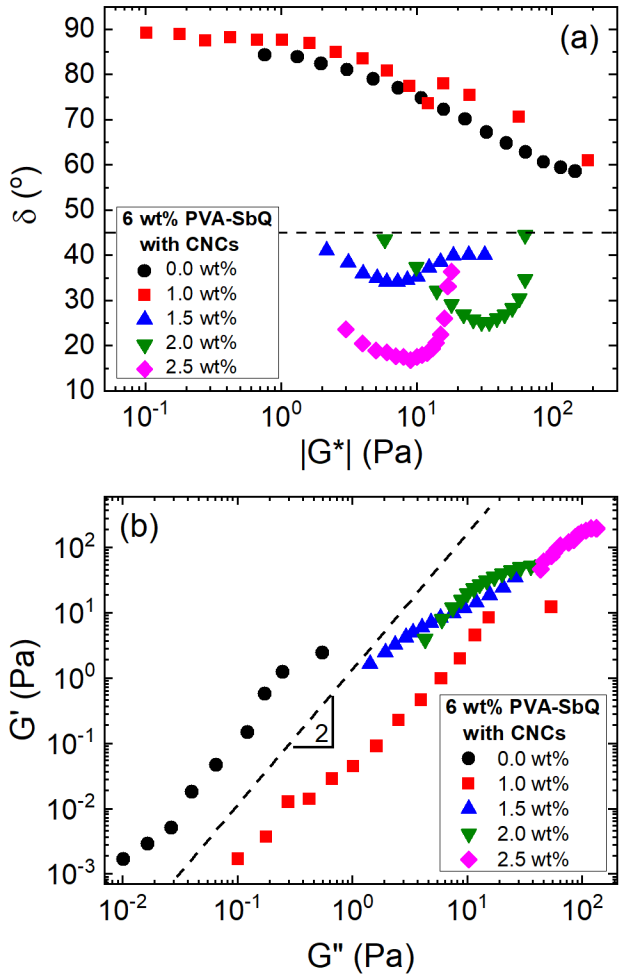

Figure 4. (a) Van Gurp-Palmen plot (δ vs. |G*|) and (b) Cole-Cole plot (G' vs. G") for 6 wt% PVA-SbQ with added CNCs, used to determine the onset of percolation behavior (data sets labeled and color-coded). The solid line in (a) indicates the criteria for percolation (δ < 45°), while the dashed line in (b) depicts a slope of 2 corresponding to the slope of the homogenous polymer network.

A van-Gurp Palmen plot is presented in **Figure 4a**. For neat PVA-SbQ and with 1 wt% CNCs, δ begins at ~90° (indicating the dominance of viscous behavior) at low |G*| and approaches 60° at high |G*|. As both these values are much higher than 45°, which is the threshold δ for percolation, this suggests the absence of a percolated network at low CNC loadings. However, upon addition of 1.5 wt% CNC, a clear difference is observed; δ remains below 45° at all |G*|, indicating that CNCs are percolated in the aqueous PVA-SbQ solution with a threshold value between 1 to 1.5 wt%. This percolation threshold concentration is within the range of those reported in previous literature for CNC-filled systems.[73,74,76] The percolated network behavior is observed for all CNC concentrations above 1.5 wt%, as δ stays below 45°.

The percolation threshold range was further verified using a Cole-Cole plot (**Figure 4b**). For a homogenous polymer system (in this case, neat PVA-SbQ), the log-log plot of G' vs. G" at low frequency should yield a slope of 2, since G' ~ ω^2, G" ~ ω, and the ratio of the exponents (G'/G") is equal to 2. Deviation from the slope of the homogenous system, with a decrease in slope representative of system heterogeneity, is often used as a measure of network formation. The Cole-Cole plot does indeed yield

a slope of 2 for neat PVA-SbQ. The addition of 1 wt% CNC shifts the curve toward higher G" but G' is still significantly lower than G", consistent with both the frequency sweep data from **Figure 3a** and the van Gurp-Palmen plots in **Figure 4a**. However, at loadings of 1.5 wt% CNCs and higher, G' dominates over G" and the slope is reduced to 1.0-1.3, indicating the existence of a percolated network. Finally, the critical gelation concentration can be calculated using the Winter-Chambon criterion, which states that gelation parameters such as time, temperature and concentration are frequency-independent at the gel point.[77,78] Accordingly, a critical gelation concentration of ~1.5 wt CNCs% was determined based on the frequency-independence of tan δ at the gel point as shown in **Figure S6**. This is also consistent with the result shown in **Figure 3a** for the 1.5 wt% sample, where the similar slopes of the two moduli suggest the sample is in the vicinity of the gel point. Values of G' at and above the percolation threshold (≥ 1.5 wt% CNCs) also exhibit power-law scaling with increasing CNC loading in accordance with theory for entangled fibrous gels[79] (**Figure S7**), indicating that interactions between percolated CNCs and PVA-SbQ increase network stiffness by functioning as additional entanglements.

Photocrosslinking of PVA-SbQ combined with CNCs. A crosslinking reaction occurs between the SbQ moieties in PVA-SbQ after UV light exposure, as previously shown in **Scheme 1**. Precise identification of the gel point can be achieved through *in-situ* photorheology, in which G' and G" are continuously measured at a fixed frequency during the UV exposure period. **Figure 5** shows the time evolution of G' and G" at ω =10 rad/s for PVA-SbQ with varying CNC loadings exposed to 60 min of continuous UV irradiation at 10 mW/cm^2. For neat PVA-SbQ (**Figure 5a**), liquid-like behavior dominates the initial microstructure as G" is higher than G' at the onset of UV exposure. During UV exposure, both moduli start to increase, with G' increasing at a faster rate relative to G", eventually crossing over at ~15 min, beyond which G' is higher than G". The modulus crossover time (t_c) can be taken as an approximation of the gel point.[58,80] Following the crossover of G' and G'', from 15 < t < 30 min, G' and G'' continue to increase at approximately the same rate. From 30 < t < 40 min, G' exhibits a rapid increase whereas G'' begins to level off. Above t = 40 min, G' levels off to a steady state value indicating maximum conversion of SbQ to its photocrosslinked form. This sigmoidal-like profile observed in **Figure 5a** for neat PVA-SbQ is in qualitative agreement with the

three-stage transition during PVA-SbQ photodimerization obtained by QCM.[34]

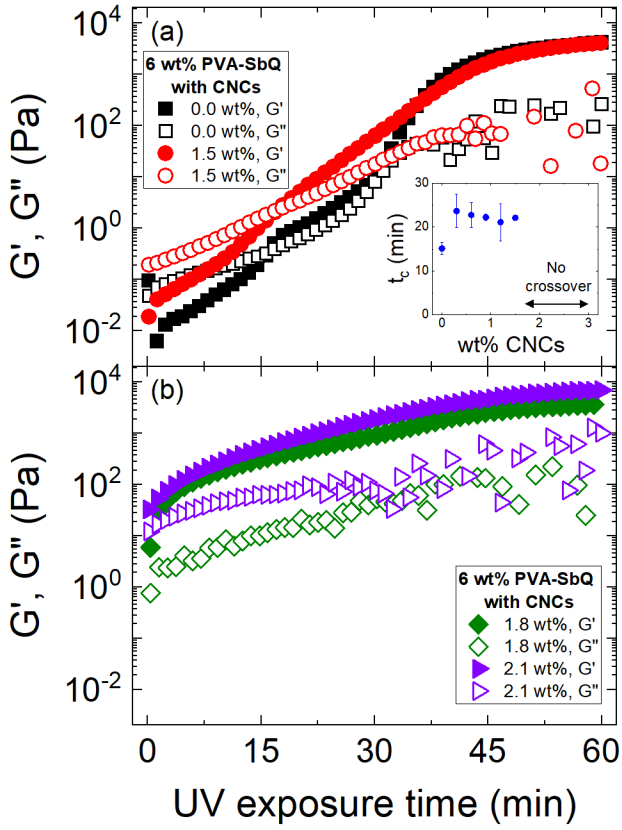

Figure 5. Representative time sweep results for 6 wt% PVA-SbQ with added CNCs (0 and 1.5 wt% in (a), 1.8 and 2.1 wt% in (b)) under 10 mW/cm^2 continuous UV illumination (data sets labeled and color-coded). Inset in (a) shows the dependence of modulus crossover time (t_c) on CNC loading, with error bars representing the standard error from duplicate measurements.

Initial liquid-like behavior followed by gelation is also observed for systems containing up to 1.5 wt% CNCs (**Figure 5a**); interestingly, t_c values for 0.3-1.5 wt% CNCs were

higher than those for neat PVA-SbQ, as presented in the **Figure 5a inset**, consistent with other reports that claim the inclusion of nanofillers slows down polymer photocrosslinking.[57,58] This observed increase in t_c with CNC loading could be due to the higher initial solution viscosities and/or CNCs initially impeding SbQ chemical crosslinking. This result is also in agreement with the work of Adibnia *et al.*[81] examining the effects of silica nanoparticles on the chemical crosslinking kinetics of polyacrylamide hydrogels. The authors conclude that increasing nanoparticle surface area (through either decreasing their size or increasing their concentration) increases polymer adsorption and delays network formation by decreasing the concentration of free polymer available for crosslinking. Further increasing the CNC concentration to 1.8 and 2.1 wt% CNCs (**Figure 5b**), results in G' exceeding G" throughout the experiment and a lack of a modulus crossover due to the material exhibiting gel-like behavior prior to UV light exposure. For all concentrations, continued UV exposure after the gel point results in further microstructural development, with G' becoming several orders of magnitude higher than G".

The gel microstructures after 60 min of UV light exposure were characterized

through frequency sweeps (**Figure 6a**). For both the neat and CNC-filled systems, G' and G" display frequency-independence, confirming that the final microstructure is a fully crosslinked gel. To elucidate the effect of CNC fillers on the mechanical strength of the composite gels, the average G' values after 60 min of UV exposure (at ω = 10 rad/s) are plotted relative to CNC content in **Figure 6b**. G' is relatively independent of concentration below 1.5 wt% CNCs, fluctuating between 3500 and 4500 Pa with no apparent trends. However, a sharp increase in G' is observed at CNC concentrations higher than 1.5 wt%. G' increases to 6400 Pa for systems containing 1.8 wt% CNCs, followed by subsequent increases to 7200 Pa and 8600 Pa for loadings of 2.1 wt% and 2.5 wt% CNCs respectively. At the maximum loading (2.5 wt%), this corresponds to a ~120% increase in G', suggesting that CNCs are providing a reinforcing effect.

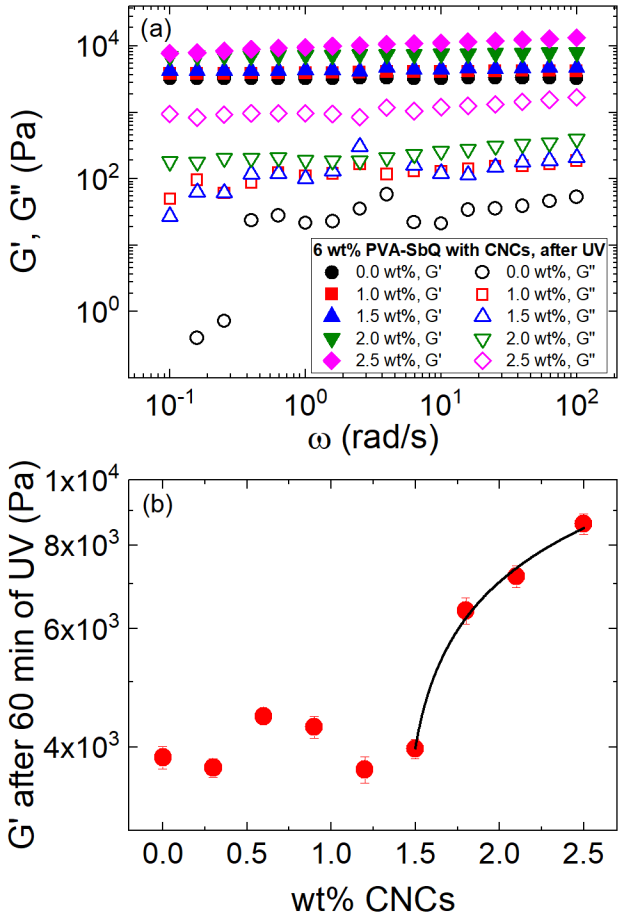

Figure 6. (a) Frequency (ω) sweep results and (b) average storage modulus (G') for 6 wt% PVA-SbQ filled with varying amounts of CNCs (wt%) after 1 h of UV exposure at 10 mW/cm^2. The black line in (b) depicts the fit of the percolation model (Equation 2) to the data. Error bars represent the standard error from duplicate measurements.

The reinforcing effect of CNCs in photocrosslinked PVA-SbQ gels can be directly related to the percolation mechanism established for these materials prior to UV

exposure. The sharp transition in G' observed in **Figure 6b** occurs because above a critical concentration, finite CNCs transition to a new state wherein clusters of CNCs interact with PVA-SbQ to span the entire network. The network of CNCs adds to the elasticity of the PVA-SbQ network, resulting in higher G' values due to the increased ability to transmit stresses across the system. The microstructure formed after UV exposure, therefore, once again resembles a percolated network. The critical concentration required to achieve mechanical percolation in the polymer nanocomposite can be calculated using the percolation model presented in Equation 2:

$$G' = a\,(m - m_c)^{\beta} \qquad (2)$$

where a is a scalar prefactor, m is the mass fraction of cellulose nanocrystals, m_c is the mass fraction required for percolation within the polymer nanocomposite, and β is an exponent at percolation.[76,82,83] This equation can only be applied near the percolation threshold.[76] Upon fitting the post-exposure G' data from **Figure 6b** for 1.5-2.5 wt% CNCs, we obtained values for a, m_c and β of 32800 ± 13700 Pa, 0.0141 ± 7E-4, and 0.30 ± 0.09, respectively (R^2 = 0.99). This m_c value of 0.0141 (or 1.41 wt%) very closely matches the percolation threshold for CNCs in 6 wt% PVA-SbQ established prior to UV

exposure (1.5 wt%).

Based on the results from our characterization, we propose a mechanism for how CNCs are likely interacting with PVA-SbQ during the photocrosslinking process (**Scheme 2**). PVA-SbQ polymer chains are mobile prior to CNC addition (entanglements not shown in **Scheme 2** for clarity). Upon addition of CNCs (which contain surface-bound water) above the rheological percolation threshold of 1.5 wt%, a sample-spanning network is formed due to attractive electrostatic interactions between positively-charged SbQ moieties and negatively-charged CNCs. The percolated network structure is maintained during photocrosslinking of PVA-SbQ, resulting in the formation of a densely interconnected gel structure which contains covalent bonds between SbQ moieties.

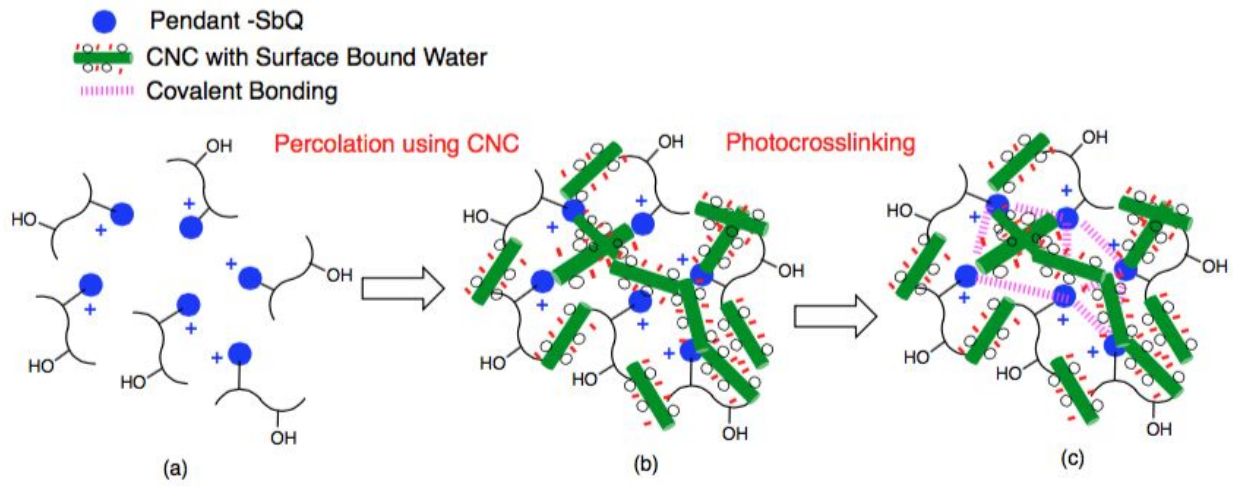

Scheme 2. Illustration of structure development in CNC/PVA-SbQ nanocomposites (proportions not drawn to scale). A percolated microstructure is first achieved through addition of negatively charged CNCs (containing surface-bound water) to positively-charged PVA-SbQ; the percolated network is maintained during covalent crosslinking of the SbQ moieties under UV exposure, resulting in a densely interconnected gel structure.

We end by considering the prospects of PVA-SbQ systems reinforced with CNCs. First, there is great promise in the formulation of inks for 3D-printable nanocomposites,[84,85] which can be tailored to exhibit a range of rheological behaviors. In turn, they allow for fitting to the demands of different extrusion systems. Moreover, UV irradiation can be applied during or after extrusion to further solidify the system and

to gain enhanced mechanical strength, especially given the presence of CNCs. Additionally, PVA-SbQ films subjected to varying degrees of UV crosslinking affords control over glass transition temperatures, most useful in coatings and membranes, which benefit from the presence of CNC and its ability to improve in-plane and out-of-plane elastic moduli. In accordance to the influence of physical and chemical crosslinks, it is possible to tune the free volume throughout the amorphous and crystalline regions of the system, most useful in regulating the transport properties, for example for oxygen and water vapor.[86] Advanced systems may exploit the presence of CNC and its interactions with PVA-SbQ, for example, for the immobilization of drugs and controlled release,[87] which can be tuned by chemical and physical coupling in photosensitive systems.

CONCLUSIONS

We report how CNC nanofillers interact with aqueous PVA-SbQ and modulate the photocrosslinking kinetics and storage moduli of the resulting nanocomposite hydrogels. Steady-shear rheological measurements of PVA-SbQ resemble those of

neutral polymers and entanglement was observed at ~4.8 wt%. Addition of CNCs to 6 wt% PVA-SbQ shows Newtonian flow behavior at low concentrations with strong deviations occurring for concentrations above 1.5 wt%, which is attributed to formation of a percolated network by CNCs with PVA-SbQ. Percolation was confirmed using van Gurp-Palmen and Cole-Cole plots and a rheological percolation threshold of 1.5 wt% CNCs was identified. *In-situ* photocrosslinking experiments of CNC-filled PVA-SbQ systems reveal that the presence of CNCs affects the gel time and ultimate storage moduli. Values of G' after 60 min of UV exposure at 10 mW/cm^2 show a sharp increase above 1.5 wt% CNCs, confirming that CNCs remain percolated in the photocrosslinked material. The increase in G' upon addition of 2.5 wt% CNCs was approximately 120% relative to photocrosslinked neat PVA-SbQ, confirming that CNCs provide a reinforcing effect in this photocrosslinkable system. Our results highlight the complexities of interactions between photosensitive polymers and nanofillers before, during, and after photocrosslinking and can be used to guide the engineering of biocompatible polymer nanocomposites for improved mechanical integrity.

CONFLICTS OF INTEREST

There are no conflicts of interest to declare.

ACKNOWLEDGEMENTS

RDC gratefully acknowledges financial support from the NSF Graduate Research Fellowship and the GAANN Fellowship in Molecular Biotechnology.

AUTHOR INFORMATION

The contact information for all authors is as follows:

Ria D. Corder: rcdomier@ncsu.edu

Prajesh Adhikari: padhika@ncsu.edu

Michael C. Burroughs: mcburroughs@ucsb.edu

Orlando J. Rojas: orlando.rojas@ubc.ca

Saad A. Khan: khan@eos.ncsu.edu

SUPPORTING INFORMATION

Images of dilute CNC dispersions with and without PVA-SbQ, calculation of the theoretical hydrodynamic radius for CNCs using the Stokes-Einstein equation and Kirkwood-Riseman theory, steady-shear rheology of CNC dispersions, calculation of intrinsic viscosity using the Huggins equation, CNC aspect ratio calculation using Simha's equation, complete frequency sweep and complex viscosity data for 6 wt% PVA-SbQ solutions containing dispersed CNCs, power-law model fitting of complex viscosity data for 6 wt% PVA-SbQ solutions containing dispersed CNCs, steady-shear rheology for 6 wt% PVA-SbQ solutions containing dispersed CNCs and Hershel-Bulkley

model fitting, approximation of the gel point concentration of CNCs in 6 wt% PVA-SbQ using the Winter-Chambon criterion, G' scaling with CNC loading prior to photocrosslinking.

REFERENCES

1 C. L. Kim and D. E. Kim, *Sci. Rep.*, 2017, **7**, 1–11.

2 D. Moreau, C. Chauvet, F. Etienne, F. P. Rannou and L. Corté, *Proc. Natl. Acad. Sci.*, 2016, **113**, 13295–13300.

3 J. Yang, R. Bai, B. Chen and Z. Suo, *Adv. Funct. Mater.*, 2020, **30**, 1901693.

4 H. Yuk, T. Zhang, S. Lin, G. A. Parada and X. Zhao, *Nat. Mater.*, 2016, **15**, 190–196.

5 C. D. Spicer, *Polym. Chem.*, 2020, **11**, 184–219.

6 Z. Chen, D. Zhao, B. Liu, G. Nian, X. Li, J. Yin, S. Qu and W. Yang, *Adv. Funct. Mater.*, 2019, **29**, 1900971.

7 Y. He, F. Yang, H. Zhao, Q. Gao, B. Xia and J. Fu, *Sci. Rep.*, 2016, **6**, 29977.

8 L. Ouyang, C. B. Highley, C. B. Rodell, W. Sun and J. A. Burdick, *ACS Biomater. Sci. Eng.*, 2016, **2**, 1743–1751.

9 S. Jiang, S. Liu and W. Feng, *J. Mech. Behav. Biomed. Mater.*, 2011, **4**, 1228–1233.

10 E. A. Kamoun, X. Chen, M. S. Mohy Eldin and E. R. S. Kenawy, *Arab. J. Chem.*, 2015, **8**, 1–14.

11 S. Pedron, A. M. Pritchard, G. A. Vincil, B. Andrade, S. C. Zimmerman and B. A. C. Harley, *Biomacromolecules*, 2017, **18**, 1393–1400.

12 A. M. Kloxin, A. M. Kasko, C. N. Salinas and K. S. Anseth, *Science*, 2009, **324**, 59–63.

13 M. Zhong, Y.-T. Liu, X.-Y. Liu, F.-K. Shi, L.-Q. Zhang, M.-F. Zhu and X.-M. Xie, *Soft Matter*, 2016, **12**, 5420–5428.

14 M. Zhong, F. K. Shi, Y. T. Liu, X. Y. Liu and X. M. Xie, *Chin. Chem. Lett.*, 2016, **27**, 312–316.

15 A. Sannino, C. Demitri and M. Madaghiele, *Materials*, 2009, **2**, 353–373.

16 S. M. F. Kabir, P. P. Sikdar, B. Haque, M. A. R. Bhuiyan, A. Ali and M. N. Islam, *Prog. Biomater.*, 2018, **7**, 153–174.

17 C. Chang and L. Zhang, *Carbohydr. Polym.*, 2011, **84**, 40–53.

18 C. C. Piras, S. Fernández-Prieto and W. M. De Borggraeve, *Biomater Sci*, 2017, **5**, 1988–1992.

19 N. Bhattarai, J. Gunn and M. Zhang, *Adv. Drug Deliv. Rev.*, 2010, **62**, 83–99.

20 C. M. Valmikinathan, V. J. Mukhatyar, A. Jain, L. Karumbaiah, M. Dasari and V. R. Bellamkonda, *Soft Matter*, 2012, **8**, 1964–1976.

21 P. Jaipan, A. Nguyen and R. J. Narayan, *MRS Commun.*, 2017, **7**, 416–426.

22 T. M. Valentin, S. E. Leggett, P.-Y. Chen, J. K. Sodhi, L. H. Stephens, H. D. McClintock, J. Y. Sim and I. Y. Wong, *Lab Chip*, 2017, **17**, 3474–3488.

23 E. M. Ahmed, *J. Adv. Res.*, 2015, **6**, 105–121.

24 A. K. Higham, C. A. Bonino, S. R. Raghavan and S. A. Khan, *Soft Matter*, 2014, **10**, 4990–5002.

25 C. A. Bonino, J. E. Samorezov, O. Jeon, E. Alsberg and S. A. Khan, *Soft Matter*, 2011, **7**, 11510.

26 R. Liu, Y. Lin, F. Hu, R. Liu, T. Ruan and G. Jiang, *Environ. Sci. Technol.*, 2016, **50**, 97–104.

27 A. Musetti, K. Paderni, P. Fabbri, A. Pulvirenti, M. Al-Moghazy and P. Fava, *J. Food Sci.*, 2014, **79**, E577–E582.

28 Y. Li, J. A. Yerian, S. A. Khan and P. S. Fedkiw, *J. Power Sources*, 2006, **161**, 1288–1296.

29 S. Senani, E. Campazzi, M. Villatte and C. Druez, *Surf. Coat. Technol.*, 2013, **227**, 32–37.

30 K. Ichimura and S. Watanabe, *J. Polym. Sci. Polym. Chem. Ed.*, 1982, **20**, 1419–1432.

31 K. Ichimura, *Makromol Chem*, 1987, **188**, 2973–2982.

32 K. Ichimura, S. Iwata, S. Mochizuki, M. Ohmi and D. Adachi, *J. Polym. Sci. Part Polym. Chem.*, 2012, **50**, 4094–4102.

33 K. Ichimura, *Bull. Chem. Soc. Jpn.*, 2017, **90**, 411–418.

34 H. Bai, J. Xu, Y. Zhang, X. Liu and O. J. Rojas, *J. Polym. Sci. Part B Polym. Phys.*, 2015, **53**, 345–355.

35 K. Ichimura and S. Watanabe, *Chem. Lett.*, 1978, **18**, 1289–1292.

36 K. Ichimura, *J. Polym. Sci. Polym. Chem. Ed.*, 1984, **22**, 2817–2828.

37 S. RoyChoudhury, Y. Umasankar, J. D. Hutcheson, H. A. Lev-Tov, R. S. Kirsner and S. Bhansali, *Electroanalysis*, 2018, **30**, 2374–2385.

38 S. Hertzberg, E. Moen, C. Vogelsang and K. Østgaard, *Appl. Microbiol. Biotechnol.*, 1995, **43**, 10–17.

39 H. Bai, Y. Sun, J. Xu, W. Dong and X. Liu, *Carbohydr. Polym.*, 2015, **115**, 422–431.

40 J. Yang and C. Han, *ACS Appl. Mater. Interfaces*, 2016, **8**, 25621–25630.

41 Q. Chen, S. Gong, J. Moll, D. Zhao, S. K. Kumar and R. H. Colby, *ACS Macro Lett.*, 2015, **4**, 398–402.

42 J. Yang, C. R. Han, X. M. Zhang, F. Xu and R. C. Sun, *Macromolecules*, 2014, **47**, 4077–4086.

43 T. Zhang, T. Zuo, D. Hu and C. Chang, *ACS Appl. Mater. Interfaces*, 2017, **9**, 24230–24237.

44 E. S. Dragan, *Chem. Eng. J.*, 2014, **243**, 572–590.

45 P. Matricardi, C. Di Meo, T. Coviello, W. E. Hennink and F. Alhaique, *Adv. Drug Deliv. Rev.*, 2013, **65**, 1172–1187.

46 J. P. F. Lagerwall, C. Schütz, M. Salajkova, J. Noh, J. Hyun Park, G. Scalia and L. Bergström, *NPG Asia Mater.*, 2014, **6**, e80.

47 C. Honorato-Rios, C. Lehr, C. Schütz, R. Sanctuary, M. A. Osipov, J. Baller and J. P. F. Lagerwall, *NPG Asia Mater.*, 2018, **10**, 455–465.

48 Y. Boluk, L. Zhao and V. Incani, *Langmuir*, 2012, **28**, 6114–6123.

49 Z. Hu, E. D. Cranston, R. Ng and R. Pelton, *Langmuir*, 2014, **30**, 2684–2692.

50 R. Bardet, N. Belgacem and J. Bras, *ACS Appl. Mater. Interfaces*, 2015, **7**, 4010–4018.

51 H. Oguzlu and Y. Boluk, *Cellulose*, 2017, **24**, 131–146.

52 N. Cohen, G. Ochbaum, Y. Levi-Kalisman, R. Bitton and R. Yerushalmi-Rozen, *ACS Appl. Polym. Mater.*, 2020, **2**, 732–740.

53 R. Blanchard, E. O. Ogunsona, S. Hojabr, R. Berry and T. H. Mekonnen, *ACS Appl. Polym. Mater.*, 2020, **2**, 887–898.

54 S. Pruksawan, S. Samitsu, Y. Fujii, N. Torikai and M. Naito, *ACS Appl. Polym. Mater.*, 2020, **2**, 1234–1243.

55 S. Zhang, D. Huang, H. Lin, Y. Xiao and X. Zhang, *Biomacromolecules*, 2020, **21**, 2400–2408.

56 N. B. Palaganas, J. D. Mangadlao, A. C. C. de Leon, J. O. Palaganas, K. D. Pangilinan, Y. J. Lee and R. C. Advincula, *ACS Appl. Mater. Interfaces*, 2017, **9**, 34314–34324.

57 B.-S. Chiou, S. R. Raghavan and S. A. Khan, *Macromolecules*, 2001, **34**, 4526–4533.

58 R. D. Corder, J. C. Tilly, W. F. Ingram, S. Roh, R. J. Spontak and S. A. Khan, *ACS Appl. Polym. Mater.*, 2020, **2**, 394–403.

59 R. Hidalgo-Álvarez, A. Martín, A. Fernández, D. Bastos, F. Martínez and F. J. de las Nieves, *Adv. Colloid Interface Sci.*, 1996, **67**, 1–118.

60 M. Rubinstein and R. H. Colby, *Polymer Physics*, Oxford University Press, New York, 2003.

61 A. V. Dobrynin, R. H. Colby and M. Rubinstein, *Macromolecules*, 1995, **28**, 1859–1871.

62 M. Rubinstein, R. H. Colby and A. V. Dobrynin, *Phys. Rev. Lett.*, 1994, **73**, 2776–2779.

63 C. D. Boris and H. R. Colby, *Macromolecules*, 1998, **31**, 5746–5755.

64 B. Briscoe, P. Luckham and S. Zhu, *Polymer*, 2000, **41**, 3851–3860.

65 H. Chang, J. Luo, A. A. Bakhtiary Davijani, A. T. Chien, P. H. Wang, H. C. Liu and S. Kumar, *ACS Appl. Mater. Interfaces*, 2016, **8**, 5768–5771.

66 R. Tantra, P. Schulze and P. Quincey, *Particuology*, 2010, **8**, 279–285.

67 M.-C. Li, Q. Wu, K. Song, S. Lee, Y. Qing and Y. Wu, *ACS Sustain. Chem. Eng.*, 2015, **3**, 821–832.

68 D. B. Genovese, *Adv. Colloid Interface Sci.*, 2012, **171–172**, 1–16.

69 A. M. Wierenga and A. P. Philipse, *Colloids Surf. Physicochem. Eng. Asp.*, 1998, **137**, 355–372.

70 Q. Zhang, F. Fang, X. Zhao, Y. Li, M. Zhu and D. Chen, *J. Phys. Chem. B*, 2008, **112**, 12606–12611.

71 O. Valentino, M. Sarno, N. G. Rainone, M. R. Nobile, P. Ciambelli, H. C. Neitzert and G. P. Simon, *Phys. E Low-Dimens. Syst. Nanostructures*, 2008, **40**, 2440–2445.

72 P. Pötschke, M. Abdel-Goad, I. Alig, S. Dudkin and D. Lellinger, *Polymer*, 2004, **45**, 8863–8870.

73 D. Bagheriasl, P. J. Carreau, B. Riedl, C. Dubois and W. Y. Hamad, *Cellulose*, 2016, **23**, 1885–1897.

74 M. R. Kamal and V. Khoshkava, *Carbohydr. Polym.*, 2015, **123**, 105–114.

75 D. Wu, L. Wu, Y. Sun and M. Zhang, *J. Polym. Sci. Part B Polym. Phys.*, 2007, **45**, 3137–3147.

76 N. E. Marcovich, M. L. Auad, N. E. Bellesi, S. R. Nutt and M. I. Aranguren, *J. Mater. Res.*, 2006, **21**, 870–881.

77 F. Chambon and H. H. Winter, *J. Rheol.*, 1987, **31**, 683–697.

78 H. H. Winter and F. Chambon, *J. Rheol.*, 1986, **30**, 367–382.

79 R. J. Hill, *Biomacromolecules*, 2008, **9**, 2963–2966.

80 J. C. Tilly, A. K. Pervaje, D. L. Inglefield, E. E. Santiso, R. J. Spontak and S. A. Khan, *ACS Omega*, 2019, **4**, 932–939.

81 V. Adibnia, S. M. Taghavi and R. J. Hill, *Rheol. Acta*, 2017, **56**, 123–134.

82 S. J. Chin, S. Vempati, P. Dawson, M. Knite, A. Linarts, K. Ozols and T. McNally, *Polymer*, 2015, **58**, 209–221.

83 C. M. Macosko, *Rheology: Principles, Measurements, and Applications*, John Wiley & Sons, Hoboken, 1994.

84 Z. Viskadourakis, G. Perrakis, E. Symeou, J. Giapintzakis and G. Kenanakis, *Appl. Phys. A*, 2019, **125**, 159.

85 G. Chinga-Carrasco, *Biomacromolecules*, 2018, **19**, 701–711.

86 J. Wang, D. J. Gardner, N. M. Stark, D. W. Bousfield, M. Tajvidi and Z. Cai, *ACS Sustain. Chem. Eng.*, 2018, **6**, 49–70.

87 P. Mena-Giraldo, S. Pérez-Buitrago, M. Londoño-Berrío, I. C. Ortiz-Trujillo, L. M. Hoyos-Palacio and J. Orozco, *Sci. Rep.*, 2020, **10**, 2110.

TABLE OF CONTENTS FIGURE

We examine how cellulose nanocrystals affect the rheology of a photoactive poly (vinyl alcohol) derivative before, during, and after photocrosslinking.